Heatmap-Based Similarity Mapping and Real-Gas Model Selection for sCO_2 Turbomachinery

Seungkyu Lee [a], Jeong Ik Lee[a*]
[a]*Dept. Nuclear & Quantum Eng., KAIST, 373-1, Guseong-dong, Yuseong-gu, Daejeon, 305-701, Republic of Korea*
[*]*Corresponding author: jeongiklee@kaist.ac.kr*

Keywords : sCO_2 Brayton cycle, Turbomachinery map, Real-gas model similitude method, Resolution baseline

1. Introduction

Nuclear propulsion concept emerged as a candidate for decarbonization of marine transport since it can provide high energy density and long endurance without refueling. A practical nuclear powered ship must satisfy various power demands such as startup & shutdown, port operation, and canal passage scenarios [1]. These requirements lead to the turbomachinery operating under various off-design conditions driven by changes in shaft power demand. For such scenarios, it is important to predict the off-design behavior across a wide range of inlet states, mass flow rates and operating speeds. This motivates extensive experimental campaigns that generate large datasets of operating points. While abundant data are valuable, dense point performance representation could be difficult to interpret. Therefore, a new compact and reproducible presentation method is needed while preserving the performance data, remain readable under large dataset, and support objective comparison across different modeling assumptions.

Another problem occurs when the working fluid exhibits nonlinearity in thermodynamic properties. Supercritical CO_2 (sCO_2) near the critical point is a representative fluid, and ideal gas assumptions are often invalid [2]. Several real gas models have been proposed by adopting compressibility factor, specific heat ratio, and isentropic exponent [3], [4], [5]. So, it is important to select real gas models providing the most consistent collapse of the off-design dataset in a non-dimensional domain.

This study proposes a methodology to represent large turbomachinery datasets in a non-dimensional similarity domain using heatmap based cell aggregation, and to select an appropriate real gas similitude model using a variation parameter, coefficient of variation (CoV) [6]. A key aspect is that CoV in a cell has not solely occurred by real gas model mismatch. Even a perfectly collapsed data can exhibit nonzero CoV when the domain is discretized into finite size cells because the underlying performance surface varies within each cell. To avoid mistaking grid size effects errors, the minimum CoV that must occur simply because each cell has a finite size is calculated. By fitting a small local plane to the cell-averaged map, the observed CoV to this minimum "baseline" are compared. The model that yields the smallest ratio can be regarded as the most suitable for representing the off-design performance of the sCO_2 turbine.

2. Methods and Results

2.1 Experimental dataset from the KAIST ABC test loop radial turbine

The experimental dataset used in this study was obtained from the radial turbine installed in the Autonomous Brayton Cycle test loop at KAIST. In this work, the loop generated a large number of turbine operating points under various inlet states and shaft speeds that are representative of frequent off-design operation expected in nuclear propulsion ship power conversion systems. The dataset was consolidated to form large operating points from various test campaigns.

During testing, the turbine mass flow rate was regulated using electrically actuated valves located on the compressor inlet & outlet, and turbine bypass lines. Turbine inlet temperature was controlled by an electric cartridge heater, while turbine inlet pressure was adjusted by inventory control using a charging line connected to a high pressure CO_2 storage tank. Turbine operating signals such as rotational speed and inlet states were measured every 0.1s, and averaged 10 samples into one data point. To ensure data consistency, points associated with unstable loop operation and non-steady conditions were excluded. Fig. 1 shows the range of turbine inlet states of the large dataset. Table I presents the radial turbine design point used as the reference condition for normalization and reporting key operating parameters of this paper.

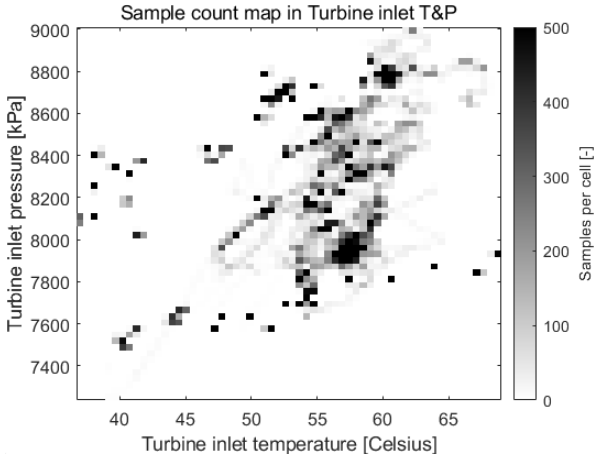

Fig. 1. Samples for cell on turbine inlet temperature and pressure

Table I: Design point of the KAIST ABC test loop turbine

Parameter	Value
Rotational speed	36,000 RPM
Mass flow rate	1.5 kg/s
Inlet total temperature	333 Kelvin
Inlet total pressure	8.9 MPa

2.2 Real-gas models for non-dimensional mapping

To construct a non-dimensional performance domain reflecting non-linear property behavior of sCO_2, this study evaluates five real gas models. Fig. 2 summarizes the relationships among the models and the corresponding definitions of the flow, speed, and head parameters. The IG model is used as a baseline similarity form, and IGZ model reflects compressibility effects with the compressibility factor [7]. Glassman and BNI models use critical temperature and critical pressure derived from isentropic sonic condition for a given inlet state rather than the static temperature and pressure [5], [8]. Here, critical refers to the sonic condition for a given inlet total state, not the thermodynamic critical point [4]. Finally, the Pham model adopts isentropic volume exponent, which can better represent real gas behavior when the pressure ratio is high.

For each experimental operating point, the required thermodynamic quantities are computed from NIST REFPROP database [9]. The resulting non-dimensional coordinates and head parameter are then used to generate the cell-based heatmaps and to quantify local collapse quality using the CoV metric described in the following sections.

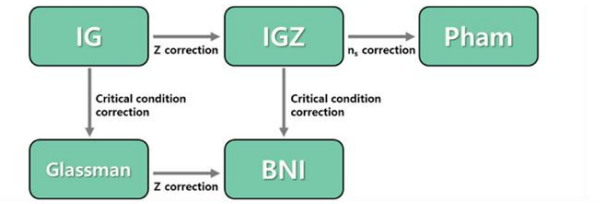

	Flow parameter	Speed parameter	Head parameter
IG	$\frac{\dot{m}\sqrt{\gamma RT}}{\gamma P}$	$\frac{N}{\sqrt{\gamma RT}}$	$\frac{\Delta H}{\gamma RT}$
IGZ	$\frac{\dot{m}\sqrt{\gamma ZRT}}{\gamma P}$	$\frac{N}{\sqrt{\gamma ZRT}}$	$\frac{\Delta H}{\gamma ZRT}$
Glassman	$\frac{\dot{m}\sqrt{\gamma RT_{cr}}}{\gamma P_{cr}}$	$\frac{N}{\sqrt{\gamma RT_{cr}}}$	$\frac{\Delta H}{\gamma RT_{cr}}$
BNI	$\frac{\dot{m}\sqrt{\gamma ZRT_{cr}}}{\gamma P_{cr}}$	$\frac{N}{\sqrt{\gamma ZRT_{cr}}}$	$\frac{\Delta H}{\gamma ZRT_{cr}}$
Pham	$\frac{\dot{m}\sqrt{n_s ZRT}}{n_s P}$	$\frac{N}{\sqrt{n_s ZRT}}$	$\frac{\Delta H}{n_s ZRT}$

Fig. 2. Five real gas models parameter equations and their relation

2.3 Cell-based heatmap representation for non-dimensional turbomachinery maps

A large turbomachinery dataset is typically visualized into a non-dimensional similarity space on the flow and speed coordinates, with performance head parameter represented by marker color or size. However, when the number of points becomes large, the plot rapidly becomes visually saturated, and the performance surface is difficult to interpret. To address these issues, this study adopts a cell-based heatmap representation that converts the dense point cloud into a structured cell.

As illustrated in Fig. 3, the non-dimensional domain defined by the selected similitude model is discretized into a uniform grid with nb x nb cells. Each experimental data point is assigned to a single cell based on its flow and speed parameters. The cell-averaged head parameter is computed and visualized as a heatmap, yielding a compact representation of the mean performance value as shown in Fig. 4. And the within-cell CoV of the head parameter is evaluated to quantify local scatter from the mean value as shown in Fig. 5.

The grid resolution is treated as an explicit design parameter of visualization. When the grid is too coarse, local variations are excessively smoothed and different operating regimes can be blended into a single cell average. Conversely, when the grid is too fine, most cells only contain few points, which increases sensitivity to measuring noise and can amplify the variance of cell statistics. Therefore, it is important to choose appropriate grid size. By combining the cell-averaged performance heatmap with the CoV map, the proposed representation enables readable visualization of large off-design datasets while retaining quantitative values.

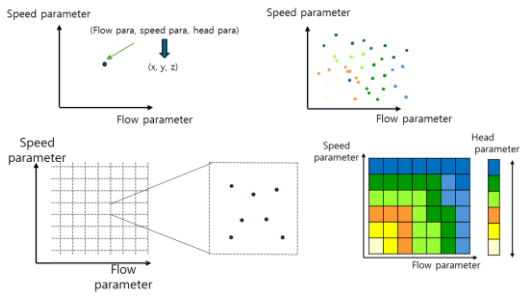

Fig. 3. Conversion methodology configuration into 2-dimensional heat map for large dataset

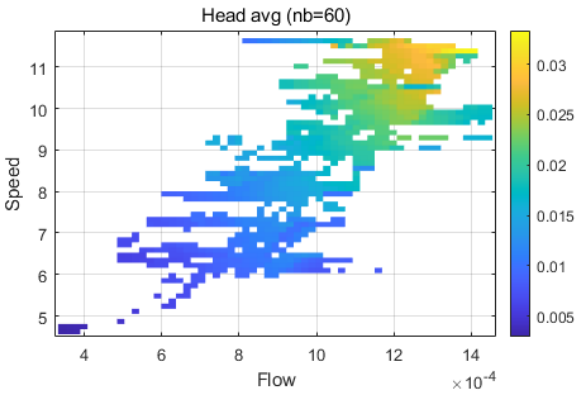

Fig. 4. Non-dimensional head parameters with IGZ model (60 x 60 cells)

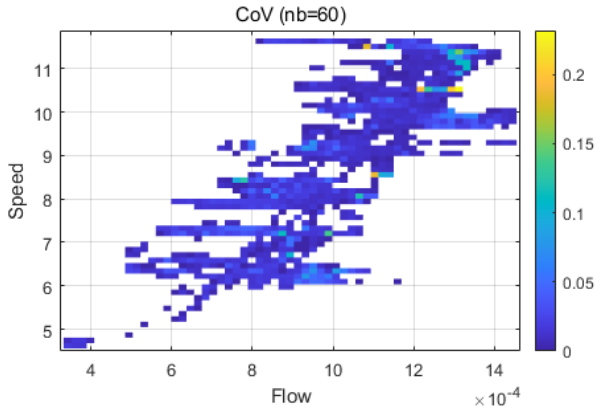

Fig. 5. CoV of Non-dimensional head parameters with IGZ model (60 x 60 cells)

2.4 Resolution aware CoV analysis and real gas model selection

After constructing the cell average heatmaps, the consistency of each similitude model is quantified using CoV computed from the within cell scatter of the non-dimensional head parameter as shown in Equation 1. The key assumption is that a proper real gas model should collapse off-design points such that neighboring locations in the non-dimensional domain represent similar speed and flow parameters and thus similar head values. To obtain a robust global metric from non-uniformly sampled points, the global CoV is evaluated as a sample count weighted RMS across populated cells as shown in Equation 2. Without sample count weighting, sparsely populated cells can influence the global score, especially when fine grids produce many low count bins.

$$CoV_c = \frac{\sigma_{z,c}}{|\bar{z}_c|} \quad (Equation\ 1)$$

$$\overline{CoV} = \sqrt{\frac{\sum_c N_c * CoV_c^2}{\sum_c N_c}} \quad (Equation\ 2)$$

Fig. 6 shows the global CoV trends decreasing as the grid resolution increases because each cell covers a smaller area of the domain. However, a smaller global CoV does not automatically imply a better similitude model, because part of the within cell scatter is unavoidable. This effect becomes more pronounced in regions where the map exhibits steep local gradients or strong curvature, depending on the real gas models and their properties. Therefore, CoV must be interpreted relative to a resolution dependent baseline rather than as an absolute indicator.

As illustrated in Fig. 7, a local micro plane is created for each cell by using neighboring cell average head parameters. This plane is utilized to estimate the local slope of the performance surface within the cell. Virtual points on the local micro plane which have same flow and speed coefficient with experiment data point are generated as shown in Equation 3. The baseline CoV are computed as Equations 4 and 5 as same as Equations 1 and 2. The CoV baseline is used as a reference for comparison against the observed CoV. Fig.8 presents the observed and baseline of CoV across grid resolution for five similitude models.

The ratio of the observed global CoV to the global baseline indicates how close each model approaches the resolution limited best case. Fig. 9 presents this ratio, enabling model ranking that is less sensitive to an arbitrary choice of grid resolution. If this ratio close to 1.0, it suggests that most of the measured scatter is consistent with finite cell size effects and thus real gas correction is proper.

For the sCO_2 ABC test loop radial turbine dataset, the IGZ model exhibits the smallest observed to baseline ratio across grid resolutions, indicating the most consistent collapse in the non-dimensional domain among the real gas model candidates. This result suggests that incorporating the compressibility factor provides a favorable balance between physical relevance, while more elaborate corrections can be sensitive to local data structure and resolution. Therefore, IGZ can be regarded as proper similitude model for compact representation of the off design sCO_2 turbine map in this study.

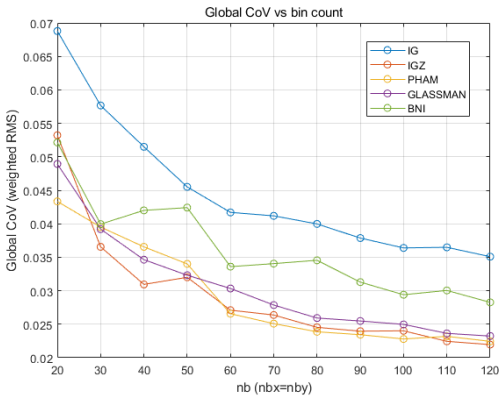

Fig. 6. Global CoV trends as the grid resolution increases

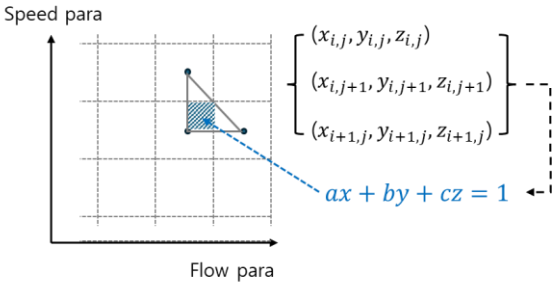

Fig. 7. Local micro plane method for estimating the cell size induced CoV baseline

$$ax + by + cz_{ideal} = 1 \ (Equation\ 3)$$

$$CoV_{c,baseline} = \frac{\sigma_{c,z,ideal}}{|\bar{z}_{c,ideal}|} \ (Equation\ 4)$$

$$\overline{CoV_{baseline}} = \sqrt{\frac{\sum_c N_c * CoV_{c,baseline}^2}{\sum_c N_c}} \quad (Equation\ 5)$$

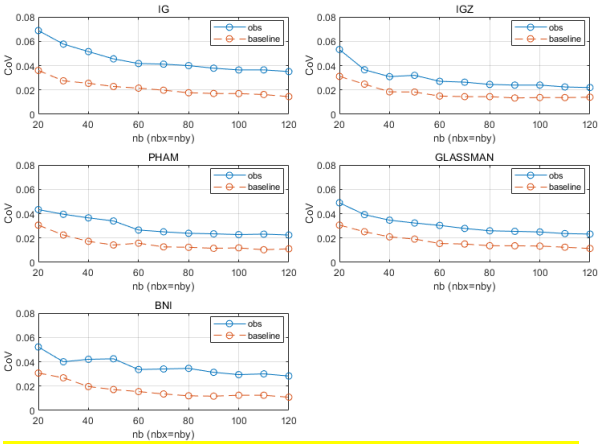

Fig. 8. Observed and baseline of CoV across grid resolution for five similitude models

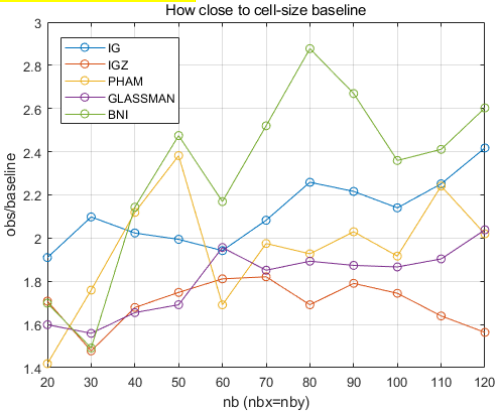

Fig. 9. Observed to baseline ratio across grid resolution for five similitude models

3. Conclusions

This paper presented a methodology to represent large turbomachinery datasets and to select an appropriate real gas similitude model in a non-dimensional domain. A large off-design experimental dataset from the KAIST ABC test loop radial turbine was transformed using five candidate real gas models and visualized with a cell based heatmap representation. The proposed heatmap approach preserved the overall topology of the performance domain while avoiding visual saturation.

To compare similitude models quantitatively, a CoV was introduced using the within cell scatter of the non-dimensional head parameter. Because the observed CoV is affected not only by similarity mismatch but also by finite cell size, a resolution induced CoV baseline was estimated from a micro plane approximation of the cell averaged surface. By evaluating the ratio of the observed global CoV to this baseline over a range of grid resolutions, the proposed framework enabled model ranking that is less sensitive to the selected bin count and that avoids over interpreting discretization artifacts as physical mismatch. For the present sCO_2 turbine dataset, the model that produced the smallest observed to floor ratio across practical grid resolutions can be regarded as the most suitable similitude model for compact and consistent off-design map representation. The proposed approach is expected to be useful for nuclear propulsion ship power conversion studies, where turbomachinery frequently operates under diverse off-design conditions and large datasets are required to support system level analysis and control design.

For the present sCO_2 radial turbine dataset from the KAIST ABC test loop, the IGZ similitude model consistently produced the lowest observed to floor ratio over practical grid resolutions, indicating that it achieves the most coherent local collapse in the non-dimensional domain among the real gas model candidates. This suggests that compressibility based correction provides an effective and robust basis for compact off-design map representation under real gas conditions.

ACKNOWLEDGEMENT

This work was supported by the National Research Foundation of Korea (NRF) grant funded by the Korea government (MSIT) (No.: RS-2024-00436693).

REFERENCES

[1] S. E. Hirdaris *et al.*, “Considerations on the potential use of Nuclear Small Modular Reactor (SMR) technology for merchant marine propulsion,” *Ocean Engineering*, vol. 79, pp. 101–130, 2014.

[2] N. D. Baltadjiev, C. Lettieri, and Z. S. Spakovszky, “An investigation of real gas effects in supercritical CO2 centrifugal compressors,” *J. Turbomach.*, vol. 137, no. 9, p. 091003, 2015.

[3] Y. Jeong, S. Son, S. K. Cho, S. Baik, and J. I. Lee, “Evaluation of supercritical CO2 compressor off-design performance prediction methods,” *Energy*, vol. 213, p. 119071, 2020, doi: 10.1016/j.energy.2020.119071.

[4] H. S. Pham *et al.*, “An approach for establishing the performance maps of the sc-CO2 compressor: Development and qualification by means of CFD simulations,” *Int. J. Heat Fluid Flow*, vol. 61, pp. 379–394, 2016, doi: 10.1016/j.ijheatfluidflow.2016.05.017.

[5] A. J. Glassman, *Turbine design and application*, vol. 290. Scientific and Technical Information Office, National Aeronautics and Space …, 1973.

[6] A. T. McKay, “Distribution of the coefficient of variation and the extended" t" distribution,” *Journal of the Royal Statistical Society*, vol. 95, no. 4, pp. 695–698, 1932.

[7] A. J. Kidnay, W. R. Parrish, and D. G. McCartney, *Fundamentals of natural gas processing*. CRC press, 2019.

[8] S. K. Roberts and S. A. Sjolander, “Effect of the specific heat ratio on the aerodynamic performance of turbomachinery,” 2005.

[9] E. W. Lemmon, I. H. Bell, M. L. Huber, and M. O. McLinden, “NIST standard reference database 23: reference fluid thermodynamic and transport properties-REFPROP, Version 10.0, National Institute of Standards and Technology,” *Standard Reference Data Program, Gaithersburg*, 2018.